16th Australasian Wind Engineering Society Workshop
Brisbane, Australia
18-19 July, 2013

Optimal Placement of Wind Turbines on Cliffs

J. Rowcroft[1], J. Sheridan[1], H.M. Blackburn[1] and D. Burton[1]

[1]Department of Mechanical and Aerospace Engineering
Monash University, Victoria 3800, Australia

Abstract

The optimal siting of wind turbines in the vicinity of cliffs is investigated, with respect to in-flow yaw angle, using wind tunnel experiments. The following flow parameters were measured above the cliff: speed-up, turbulence intensity, changes in wind direction, and the persistence of vortices shed from the crest of the cliff. These experiments demonstrate that at half a cliff height above the cliff, and that same distance down-stream of the crest, there exists an optimal region with increases in wind speed, combined with lower levels of turbulence intensity across the range of in-flow angles that were investigated. In contrast, the far wake experiences velocity deficit and an increase in turbulence intensity, when compared to the in-flow. Furthermore, vortices are shed from the down-stream reattachment region and persist beyond ten cliff heights down-stream.

Introduction

A number of operational Australian wind farms exist atop cliffs, taking advantage of the well-documented speed-up associated with flow over forward facing steps (FFSs) (Bowen and Lindley 1977), such as the Albany Wind Farm in Western Australia, pictured in Figure 1. Researchers such as Sherry et al. (2010), Castro and Dianat (1983), and Largeau and Moriniere (2006) warn of the recirculation region immediately down-stream of FFSs. Work by Kiya and Sasaki (1983) demonstrates that vortices are ejected from the recirculation region and persist down-stream. Subjecting wind turbines to the buffeting associated with these turbulent recirculations and ejections results in reduction of both instantaneous energy production, and increased fatigue loading on the structure. Pitch angles, regions of high shear, and veer (change of wind direction with height) all impart unbalanced loads onto the wind turbine.

Within the literature to date, research has predominantly considered flow over FFSs with in-flow perpendicular to the crest. Work by Rowcroft et al. (2012) examined the length of the recirculation region through a range of yaw angles using surface visualisation techniques, giving consideration to the flow structure. The current research builds onto that work by taking flow measurements above the surface. In this paper, non-zero yaw angles are considered alongside the zero-yaw base-line case. Mean reattachment length established by Rowcroft et al. (2012) are presented in Table 1.

By comparing maps of speed-up, turbulence intensity, pitch and yaw, it is possible to deduce the optimal location for wind turbines in the vicinity of straight-edged FFSs.

Yaw Angle	Mean Reattachment Length
0°	2.8*h*
20°	3.2*h*
30°	3.4*h*
40°	3.8*h*

Table 1. Mean Reattachment lengths v yaw angle for the cases examined here, first presented in Rowcroft et al. (2012).

Methodology

Measurements were conducted in the 450 kW closed circuit wind tunnel at Monash University, shown in Figure 2. The FFS models were of height h = 0.05 m, and were placed on a false floor with 3.2 m fetch, and the base 0° case extended 48h downstream. The models had end-plates extending 12h upstream. Wedges were added to the front of the base model to simulate a range of in-flow angles, θ = 0°, 20°, 30°, and 40°. The models were nominally smooth. The testing velocity was 34 ms^{-1}, corresponding to a Reynolds number of 1.0×10^5. The in-flow velocity and turbulence intensity profiles are presented in Figure 3 while the vertical profile of stream-wise integral length scales is presented in Figure 4. The integral length scales were calculated by fitting von Kármán curves to the power spectral density plots, based on the peak frequency. The method is based on that used by Hui et al. (2009). A boundary layer of thickness δ = 100 mm was generated. Thus a δ/h ratio of 2 was used. The wind tunnel flow modelled neutral atmospheric stability conditions (Cook 1978).

Figure 1. Albany Wind Farm, Western Australia. Turbines are sited near cliffs, approximately 100 m above sea-level. Photo sourced from *Tourism Western Australia*.

Figure 2. Two Cobra Probe configuration for two-dimensional traversing. Traversing vertically and in the stream-wise direction. Viewed from downstream.

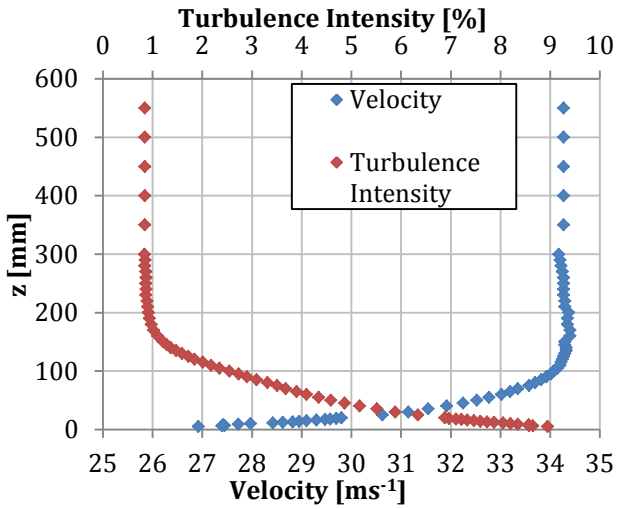

Figure 3. In-flow velocity and turbulence intensity profiles.

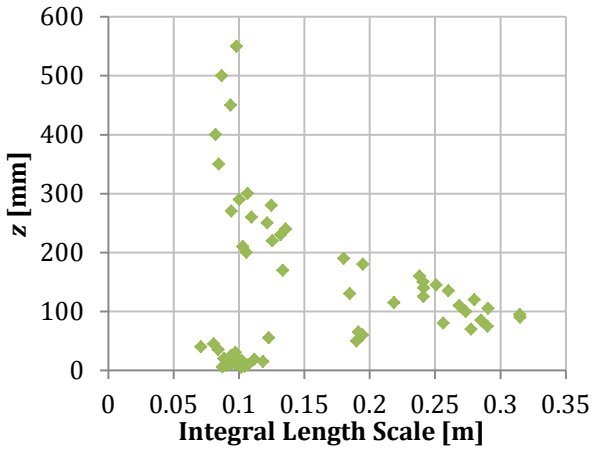

Figure 4. In-flow stream-wise integral length scales based on fitting von Kármán curves to the power spectral density plots.

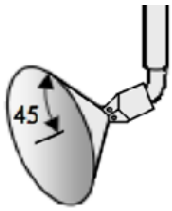

Figure 5. TFI Cobra Probe and the 45° cone of acceptance.

The region downstream of the crest of the FFS was traversed with two four-hole Cobra Probes, sampling at a frequency of 2500 Hz over a period of 180 s. The probes were spaced 50 mm apart and their heads were aligned parallel to the crest of the FFS, whilst oriented in the direction of the free-stream flow.

The capabilities of the Cobra Probes are specified in Getting Started: Series 100 Cobra Probe (Turbulent Flow Instrumentation, 2011). The probes measure three-component velocity and static pressure provided that the flow direction is within a 45° cone of acceptance, as illustrated in Figure 5.

Free-stream velocity measurements were calculated based on dynamic pressure measurements from the up-stream Pitot-Static tube. Air density was calculated based on atmospheric pressure measured in the laboratory with a *Tief Hoch* barometer, and temperature measured in the tunnel using a thermocouple.

Co-ordinates are based on a Cartesian co-ordinate system: x is the direction perpendicular to the crest of the FFS, y is the lateral direction along the crest of the FFS, and z is the vertical direction.

Results and Discussion

To determine the optimal siting of wind turbines, maximum energy output needs to be balanced against wind turbine and wind turbine component life-span. For example, unbalanced loads can cause premature failure of gearboxes, which is not a catastrophic failure of the whole wind turbine. Thus, the following considerations are presented: flow speed-up, turbulence intensity, pitch and yaw. Additionally, the location and development of coherent structures are addressed.

Speed-Up

Speed-up, S, is visualised in Figure 6, and is defined according to the following equation:

$$S = \frac{U_{Model}(x,z) / U_{Pitot,Model}}{U_{BL}(z) / U_{Pitot,BL}} \quad (1)$$

$U_{Model}(x,z)$ is the velocity at a point (x,z), according to the previously defined Cartesian co-ordinate system. $U_{Pitot,\ Model}$ is the velocity measured at the up-stream Pitot-Static tube, measured concurrently to $U_{Model}(x,z)$. $U_{BL}(z)$ is the velocity in the undisturbed boundary layer, that is, without the model in place, at $x = 0$. $U_{Pitot,\ BL}$ is the velocity measured at the up-stream Pitot-Static tube, measured concurrently to $U_{BL}(z)$.

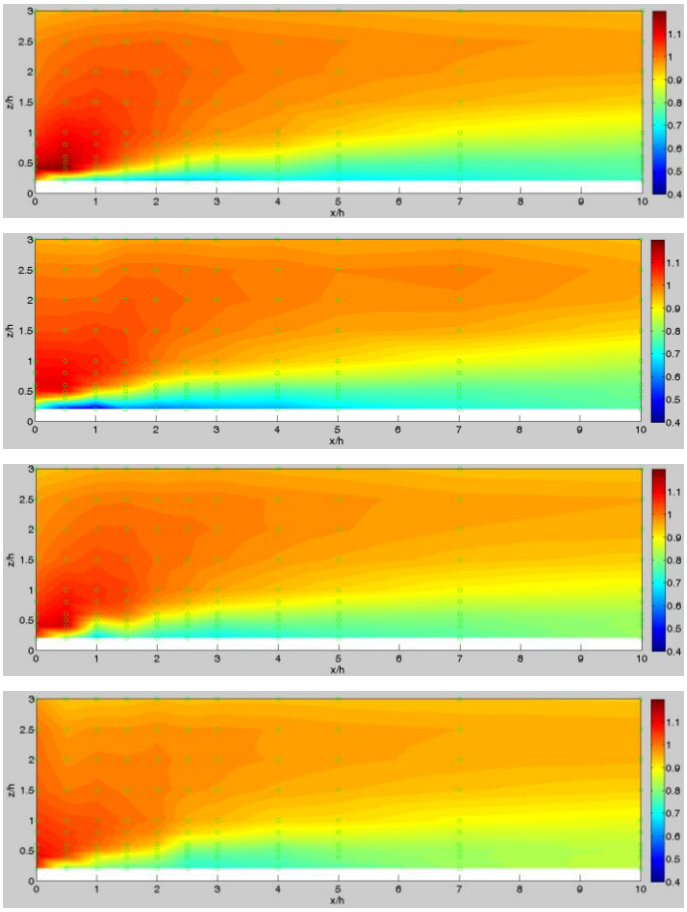

Figure 6. Map of speed-up down-stream of crest of FFS, as defined by Equation (1). From top to bottom, yaw angles are 0°, 20°, 30°, and 40°. Green circles represent measurement locations.

Maximum speed-up in each of the cases occurs between the crest and 2h downstream of the crest, and above 0.5h from the surface

of the FFS, decreasing gradually with height. As the yaw angle increases, the speed-up is less intense, but the region of increased speed-up is increased.

Note, in Figure 6, that the region of velocity deficit, that is, where speed-up is less than 1, extends into the far wake beyond x/h = 10. In contrast, speed-up dissipates to below 1 soon after x/h = 2, except in the 40° yaw angle cases, where some speed-up greater than 1 extends beyond x/h = 10, through a band between z = 2h and z = 2.75h, providing up to 1 % increase in wind speed beyond 10h downstream.

Change in Turbulence Intensity

Change in turbulence intensity, visualised in Figure 7, is defined according to the following equation:

$$TI\ Ratio = \frac{I_{uvw,Model}(x,z)}{I_{uvw,BL}(z)} \qquad (2)$$

$I_{uvw}(x,z)$ is the turbulence intensity based on the three velocity components, with the *Model* and *BL* subscripts, and the (x,z) location having the same meaning as in Equation (1).

The region of highest turbulence intensity, as shown in Figure 7, is consistent with the location of the recirculation zone through all the yaw angles examined. Beyond the recirculation region, vortices are still ejected downstream. These vortices gradually weaken, resulting in a reduction of the turbulence intensity ratio, but the turbulence intensity, even 10h downstream, is in the order of two to three times that measured in the in-flow conditions up to a height of 1.5h above the surface.

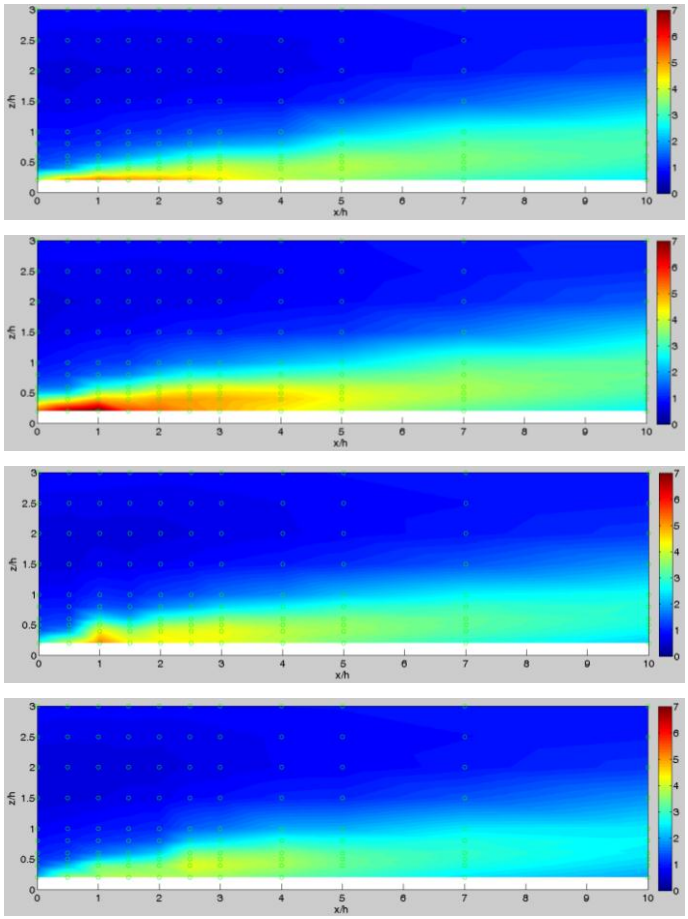

Figure 7. Map of turbulence intensity ratio down-stream of crest of FFS, as defined by Equation (2). From top to bottom, yaw angles are 0°, 20°, 30°, and 40°. Green circles represent measurement locations.

Development of Pitch and Yaw

Flow yaw angles are plotted in the colour plots in Figure 8, superimposed with a quiver plot depicting the pitch angles. Ideally, wind turbines are not subjected to large pitch angles, or variations in yaw angle as a function of height above the ground. The primary standard used in the wind energy industry to certify wind turbines is from the International Electrotechnical Commission (IEC), IEC61400-1 (2005), which requires that wind turbines be capable of operation for in-flows with pitch angle up to ±8°. At the crest and through the recirculation region, the pitch falls outside of this design envelope in each model. However, in each case, the measurements taken at 0.5h down-stream of the crest, for z > 0.5h, were within the range of 0°–4°.

The measured yaw angle and its variation with height above the surface prove to be an issue through the recirculation region, where speed-up is low, turbulence intensity is large and pitch is high. In the wake region beyond the recirculation bubble, the veer remains significant. The region up to 0.75h above the surface undergoes a strong veer, which can be seen in the 20°, 30°, and 40° models.

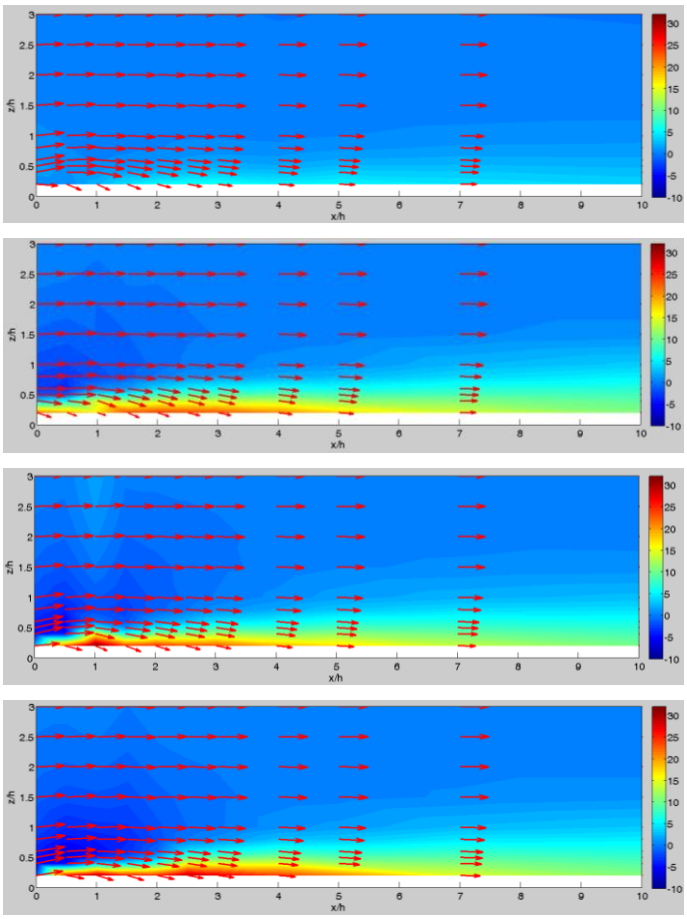

Figure 8. Map of flow yaw angles down-stream of crest of FFS, superimposed with quiver plot of pitch angles. From top to bottom, yaw angles of the models are 0°, 20°, 30°, and 40°.

Development of Coherent Structures

Figure 9 presents normalised cross-covariances from the two traversing Cobra probes. The cross-covariance is normalised against the maximum cross-covariance value obtained from the respective model.

Within the recirculation region near the crest of the FFS there is clearly an increased correlation between the two Cobra probes relative to the free-stream flow. However, this increase in correlation persists through to 10h downstream, that is, to the last

plane of measurement downstream. This shows, as Kiya and Sasaki (1983) established, that the recirculation bubble regularly bursts, shedding vortices down-stream, explaining the increases in turbulence and reduction in speed through that down-stream region.

If the persistent down-stream vortices could be broken down, the adverse down-stream turbulence intensity and veer conditions could be mitigated, but the speed-up would not increase above 1.

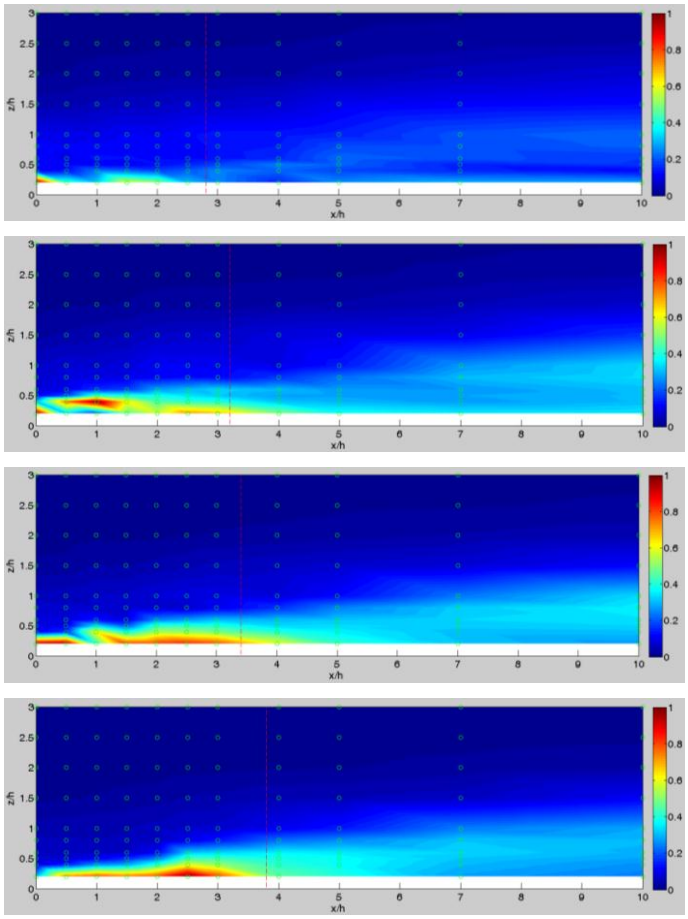

Figure 9. Plot of the maximum cross-covariances between two probes traversing 50 mm apart in the y-direction over an FFS. Data is normalised against the measured maximum cross-covariance for the case. From top to bottom, yaw angles of the models are 0°, 20°, 30°, and 40°. Green circles represent measurement locations. Vertical red dashed lines represent the mean reattachment locations.

Conclusions

The optimal location for siting wind turbines in the vicinity of a FFS has been discussed, with consideration given to speed-up, turbulence intensity, pitch and yaw angles, and to the shedding of vortices from the crest of an FFS through a range of in-flow yaw angles.

Large pitch angles are observed at the crest of the cliff, providing conditions outside of the design envelope specified in the standard IEC61400-1 (2005).

Rotors will encounter high veer, high turbulence intensity, lower wind speeds, and unfavourable shear profiles should they pass through the recirculation bubble – between the crest and 3-4 cliff heights down-stream.

Beyond 10*h* downstream of the crest, a wake profile still exists. Rotors will be subjected to reduced wind speeds, increased turbulence intensity, wind veer, and low frequency buffeting from vortex ejections from the recirculation bubble.

A region approximately 0.5*h* downstream of the crest, and above 0.5*h* above the surface provides a region with the following characteristics: increased wind speed; lowest turbulence intensity at that height, and reducing with increased height; pitch angles within the design envelope defined by the standard IEC61400-1 (2005); low wind veer; and away from the low frequency buffeting associated with shedding vortices. This location provides the optimal location for a wind turbine, providing maximal energy output, whilst minimising fatigue loading across the in-flow conditions investigated.

This work makes no consideration of lateral variations along the crest of the FFS that might be encountered due to the natural ruggedness of cliffs. Nor is the surface roughness considered. Future work will consider the effect of lateral variation along the cliff.

Acknowledgements

This research was supported under the Australian Research Council's Linkage Project funding scheme, project number LP100100746. The authors wish to acknowledge the support of industry partners Entura and Suzlon Australia.

References

Bowen, A. J. and D. Lindley (1977). "A wind tunnel investigation of the wind speed and turbulence characteristics close to the ground over various shaped escarpments." Boundary Layer Meterology **12**: 259-271.

Castro, I. P. and M. Dianat (1983). "Surface flow patterns on rectangular bodies in thick boundary layers." Journal of Wind Engineering and Industrial Aerodynamics(11): 107-119.

Cook, N. J. (1978). "Wind-tunnel simulation of the adiabatic atmospheric boundary layer by roughness, barrier and mixing-device methods." Journal of Industrial Aerodynamics **3**: 157-176.

Hui, M. C. H., A. Larsen, et al. (2009). "Wind turbulence characteristics study at the Stonecutters Bridge site: Part II: Wind power spectra, integral length scales and coherences." Journal of Wind Engineering and Industrial Aerodynamics **97**(1): 48-59.

IEC (2005). IEC 61400 Wind Turbines. Part 1: Design Requirements. Geneva, International Electrotechnical Commission.

Kiya, M. and K. Sasaki (1983). "Structure of a turbulent separation bubble." Journal of Fluid Mechanics **137**: 83-113.

Largeau, J. F. and V. Moriniere (2006). "Wall pressure fluctuations and topology in separated flows over a forward-facing step." Experiments in Fluids **42**(1): 21-40.

Rowcroft, J., J. Sheridan, et al. (2012). Surface flow visualisation over forward facing steps with varying yaw angle. The Science of Making Torque from the Wind. S. Barth. Oldenburg, Germany, ForWind.

Sherry, M., D. Lo Jacono, et al. (2010). "An experimental investigation of the recirculation zone formed downstream of a forward facing step." Journal of Wind Engineering and Industrial Aerodynamics **98**(12): 888-894.

Turbulent Flow Instrumentation (2011). Getting Started: Series 100 Cobra Probe. Victoria, Australia, Turbulent Flow Instrumentation.